Journal of
Synchrotron
Radiation

ISSN 1600-5775

Received 30 July 2013
Accepted 14 January 2014

Microfocusing options for the inelastic X-ray scattering beamline at sector 3 of the Advanced Photon Source

A. M. Alsmadi,[a,b,c]* A. Alatas,[c] J. Y. Zhao,[c] M. Y. Hu,[c] L. Yan[c] and E. E. Alp[c]

[a]Physics Department, The Hashemite University, Zarqa 13115, Jordan, [b]Physics Department, Kuwait University, 13060 Safat, Kuwait, and [c]Advanced Photon Source, Argonne National Laboratory, Argonne, IL 60439, USA. *E-mail: abdel.alsmadi@gmail.com

Synchrotron radiation from third-generation high-brilliance storage rings is an ideal source for X-ray microbeams. The aim of this paper is to describe a microfocusing scheme that combines both a toroidal mirror and Kirkpatrick–Baez (KB) mirrors for upgrading the existing optical system for inelastic X-ray scattering experiments at sector 3 of the Advanced Photon Source. *SHADOW* ray-tracing simulations without considering slope errors of both the toroidal mirror and KB mirrors show that this combination can provide a beam size of 4.5 μm (H) × 0.6 μm (V) (FWHM) at the end of the existing D-station (66 m from the source) with use of full beam transmission of up to 59%, and a beam size of 3.7 μm (H) × 0.46 μm (V) (FWHM) at the front-end of the proposed E-station (68 m from the source) with a transmission of up to 52%. A beam size of about 5 μm (H) × 1 μm (V) can be obtained, which is close to the ideal case, by using high-quality mirrors (with slope errors of less than 0.5 μrad r.m.s.). Considering the slope errors of the existing toroidal and KB mirrors (5 and 2.9 μrad r.m.s., respectively), the beam size grows to about 13.5 μm (H) × 6.3 μm (V) at the end of the D-station and to 12.0 μm (H) × 6.0 μm (V) at the front-end of the proposed E-station. The simulations presented here are compared with the experimental measurements that are significantly larger than the theoretical values even when slope error is included in the simulations. This is because of the experimental set-up that could not yet be optimized.

Keywords: inelastic X-ray scattering; microfocusing options; KB mirrors; *SHADOW* ray tracing.

1. Introduction

Inelastic X-ray scattering (IXS) is a powerful technique capable of probing the dynamic behavior and electronic structure of materials. At sector 3-ID at the Advanced Photon Source (APS), three different techniques related to IXS are currently in use: coherent elastic nuclear resonant scattering (van Bürck, 1999; Sturhahn, 2004), incoherent nuclear resonant inelastic scattering (NRIXS) (Chumakov & Sturhahn, 1999; Sturhahn & Jackson, 2007), and momentum-resolved high-energy resolution inelastic X-ray scattering (Burkel, 1991). Coherent elastic nuclear resonant scattering of synchrotron radiation [also known as nuclear forward scattering or synchrotron Mössbauer spectroscopy (SMS)] probes the magnetic hyperfine interactions of particular isotopes such as ^{83}Kr, ^{57}Fe, ^{121}Eu, ^{119}Sn and ^{161}Dy in the energy range 9–26 keV depending on the nuclear resonance transition energy of each isotope. Magnetic ordering, different valence and spin states can be determined directly from SMS spectra. NRIXS is used to measure the phonon density of states and it gives a direct measure of the atomic vibration experienced by the resonant atom in its host materials. Momentum-resolved high-energy resolution inelastic X-ray scattering, on the other hand, is used to measure the dynamical structure factor of solids and liquids. From this, phonon dispersion relations, sound velocity, force constants and elastic properties of a system can be deduced.

In addition, nuclear resonant scattering techniques can be used as an excellent microscope with very high contrast imaging. Compared with other microscopic techniques, for example the X-ray *K*-edge fluorescence technique, nuclear resonant imaging yields an excellent contrast with no background (Yan *et al.*, 2012). The recent development of installing a Mössbauer microscope at sector 3 allowed us to successfully perform 5 μm spatial resolution imaging on a sub-micrometer-thick sample of ^{57}Fe (Yan *et al.*, 2012). The strength of these techniques is their selectivity to the nuclear isotope, which allows well defined sample regions of interest to be studied.

All of the above IXS-related techniques require very high energy resolution (meV monochromatization) of the incident X-ray beam (Sinn *et al.*, 2001; Toellner *et al.*, 2006; Toellner, 2000). In order to achieve this very high resolving power, the incident photon flux is highly reduced, making IXS an extremely photon-craving experimental technique in which every photon counts. In addition, for most of the recent IXS experiments, especially those performed under extreme conditions (high pressure, high and/or low temperature), an X-ray beam of micrometer size is often required (Gao *et al.*, 2009). In order to achieve pressures above 200 GPa using state-of-the-art diamond-anvil-cell technology (Mao *et al.*, 2001*a*,*b*), the sample size should be less than 10 μm. These high-pressure studies provide valuable insight into the interior of the Earth and other planets. Of course, a micrometer beam size is not only required for high-pressure experiments but also plays a key factor in many nuclear resonant imaging experiments which have applications in life sciences (Xu *et al.*, 2011) and mineral physics (Yan *et al.*, 2012). Spot sizes down to the micrometer or sub-micrometer level while maintaining the available photon flux on the sample are still one of the goals that challenge the IXS community.

Over the past decade, experimental set-ups at sector 3 have constantly been improved. These improvements have included implementation of a second undulator to increase the incoming photon flux on the sample, adding a compound refractive lens to collimate the beam (Zhao *et al.*, 2002), improvement in the energy resolutions using new high-resolution (room temperature and cryogenically cooled) monochromators (Toellner *et al.*, 2011), improvement in the analyzer efficiency and increase in their number to collect data simultaneously at different momentum transfer points, adding new Kirkpatrick–Baez (KB) mirrors and combining a toroidal and KB mirrors to provide much smaller beam sizes (Alatas *et al.*, 2011), and recent development for the integration of nuclear resonant scattering and X-ray diffraction measurements for high-pressure research (Gao *et al.*, 2009).

At the present time, a beam size of about 15 μm (H) × 10 μm (V) (full width at half-maximum, FWHM) is available at the B-station for elastic and inelastic nuclear resonant scattering experiments, with a flux of about 1.5×10^{13} photons s^{-1} eV^{-1} coming out of the high-heat-load monochromator and a flux of about 4.5×10^{9} photon s^{-1} over the 1 meV bandwidth coming out of the high-resolution monochromator. On the other hand, a beam size of about 20 μm (H) × 17 μm (V) (FWHM) with a transmission up to 70% (4×10^{9} photons s^{-1} meV^{-1}) at the C-station is available for momentum-resolved high-energy resolution inelastic X-ray scattering spectrometry (Alatas *et al.*, 2011). With these beam properties, sector 3 has been successfully used to study the dynamic behavior and electronic structure of different materials under extreme conditions. Among these successes are the direct measurement of the phonon density of states (DOS) of iron by nuclear resonant inelastic X-ray scattering to 153 GPa (Mao *et al.*, 2001) and 171 GPa (Murphy *et al.*, 2001), and the sound velocity and density relation of iron up to 100 GPa and 700 K by momentum-resolved high-energy resolution inelastic X-ray scattering (Mao *et al.*, 2012). The current set-ups allow studies at ambient/high pressure and high/low temperature, a combination of high pressure and high temperature (Gao *et al.*, 2009). However, measurement of the phonon density of states under pressure and at low temperature simultaneously has proved to be difficult, due to space limitations in placing the detectors next to the sample. However, it is possible to combine high-pressure and low-temperature set-ups for nuclear forward scattering and momentum-resolved high-energy resolution inelastic X-ray scattering experiments and this is one of the goals of the upcoming upgrade of sector 3 at the APS. Again, beam spot size down to a few micrometers plays a key factor for such measurements.

In this paper, we describe a microfocusing design that combines both a toroidal mirror and KB mirrors to be implemented with different arrangement options for sector 3 of the APS. *SHADOW* ray tracing simulations without considering slope errors of both the toroidal mirror and KB mirrors show that this combination can provide beam sizes of 4.5 μm (H) × 0.6 μm (V) (FWHM) at the end of the existing D-station (66 m from the source) with a transmission of up to 59% and a beam size of 3.7 μm (H) × 0.46 μm (V) (FWHM) in front of the proposed E-station (68 m from the source) with a transmission of up to 52%. Considering the slope errors of the existing toroidal mirror and KB mirrors that have quite high slope errors, the beam size grows to about 13.5 μm (H) × 6.3 μm (V) at the end of the D-station and to 12.0 μm (H) × 6.0 μm (V) at the front-end of the proposed E-station. At the D-station, there is enough space to install a cryostat with a possible external magnetic field. With this new set-up, experiments that combine high pressure, low temperature and an external magnetic field can be performed. In addition, with better mirrors, sub-micrometer-resolution imaging can be achieved. With these synchrotron Mössbauer and nuclear resonant incoherent X-ray imaging techniques, it is possible to image biological samples without radiation damage.

2. Optical (beam) design

The source of the sector 3 beamline is two 2.4 m-long standard APS undulators with a magnet period of 27 mm. The source size at the undulator is about 645 μm (H) × 26 μm (V) (FWHM), and the emittance is about 3.15 nm rad (X) × 2.9 × 10^{-2} nm rad (Z). The layout of the 3-ID beamline optics is shown in Fig. 1. The major optical components are a high-heat-load monochromator (HHLM) consisting of water-cooled diamond crystals, white beam slits, four different types of high-resolution monochromator (HRM) working at different energies between 9 and 26 keV, and the KB mirrors that are placed right before the sample. In addition, there is a toroidal focusing mirror (FM), a cryogenically cooled six-reflection HRM, and a 6 m-long analyzer arm equipped with four analyzers working very close to back reflection (about 89.98°), for the momentum-resolved IXS spectrometer.

The Pd-coated toroidal FM is used to focus the entire undulator beam at a specified position. Its length is 800 mm and it is located after the cryogenically cooled HRM (at

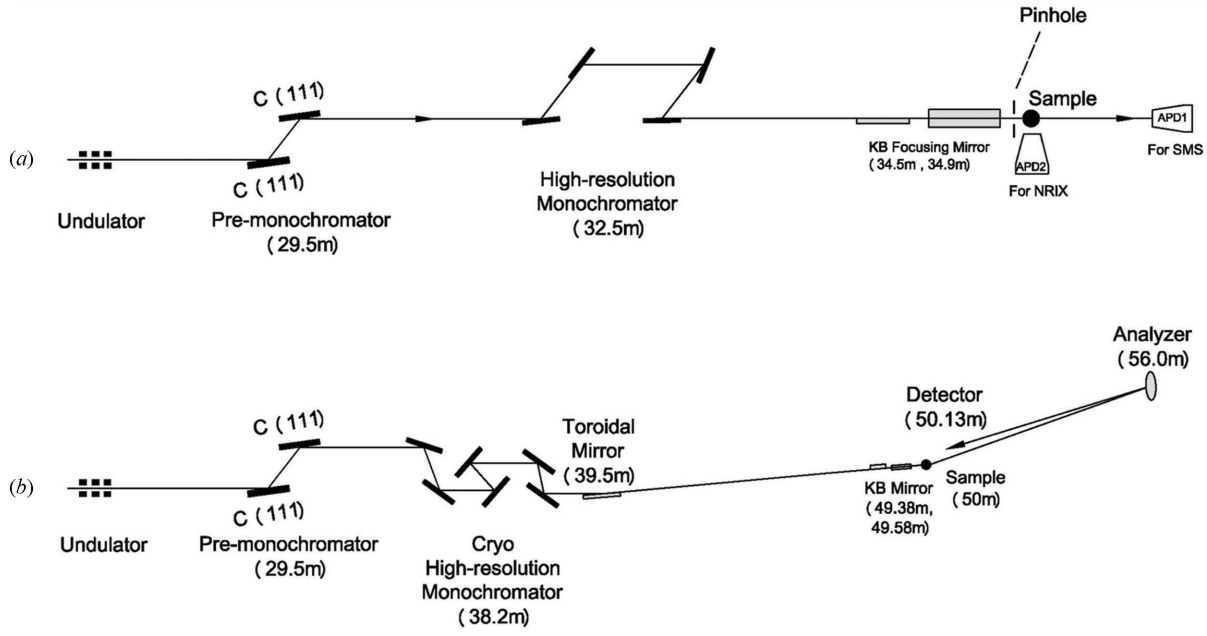

Figure 1
Basic layout of the sector 3 beamline of the APS of Argonne National Laboratory. (*a*) Positions of optical elements from the source for nuclear resonant inelastic X-ray scattering (NRIXS) and synchrotron Mössbauer spectroscopy (SMS) experiments at the B-station. (*b*) Positions of optical elements from the source for momentum-resolved IXS experiments at the C-station.

39.5 m from undulator source). The toroidal mirror is defined by two radii: the minor (also called sagittal) radius, which is fixed at 46 mm, and the major (or meridional) radius, that can take any value from 11 to 33 km. By changing the grazing incident angle and the major radius, this mirror is used to efficiently focus the entire undulator beam, both vertically and horizontally, for the experiments at the C- and D-stations. It can also be used in tandem with KB mirrors to further focus the beam by creating a secondary source. The new images of the toroidal FM are then focused to the desired size by the KB mirrors. The existing toroidal FM has a slope error of about 5 µrad r.m.s. The curvature of the mirror (meridional radius) is adjusted mechanically by a pneumatic system.

For a given grazing incident angle (θ) of the toroidal FM, the object (r) and image (r') distances are given by (Peatman, 1997; Huang *et al.*, 2008)

$$\frac{1}{r}+\frac{1}{r'}=\frac{2}{R\sin\theta} \qquad (1)$$

for the major focus and

$$\frac{1}{r}+\frac{1}{r'}=\frac{2}{\rho/\sin\theta} \qquad (2)$$

for the minor focus, where R is the major radius of the mirror and ρ is the minor radius. By changing the grazing incident angle, the horizontal and the vertical images can be moved to different positions. As a result, the required demagnification in the horizontal and vertical directions might be different. We used equations (1) and (2) to calculate the focusing conditions of the toroidal FM mirror as a function of the grazing incident angle and these calculations are also simulated using the ray-tracing software *SHADOW* in the *XOP* program package (Lai & Cerrina, 1986; Sánchez del Rio & Dejus, 2004). In order to maintain the reflectivity to an acceptable level, we choose to change the grazing angle in the range between 1.5 and 4.5 mrad. The horizontal and vertical spot sizes (FWHM) at the toroidal mirror's focus, as well as the horizontal and vertical image distances of the toroidal FM mirror, are shown as a function of the grazing incident angle in Fig. 2. For vertical image distance calculations, the major bending radius was fixed at 11779.76 m where it is close to the mechanical limit of our toroidal mirror. While the horizontal spot size decreases by increasing the grazing incident angle, the vertical spot size

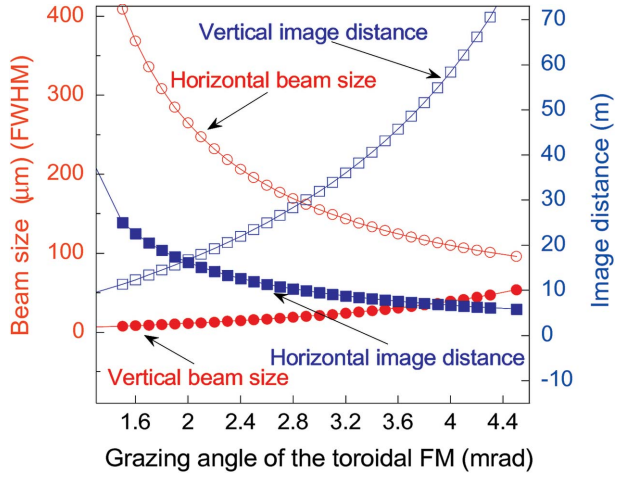

Figure 2
Horizontal (blue solid squares) and vertical (blue open squares) image distance, and horizontal (red open circles) and vertical (red solid circles) spot sizes (FWHM) of the toroidal FM mirror as a function of the grazing incident angle.

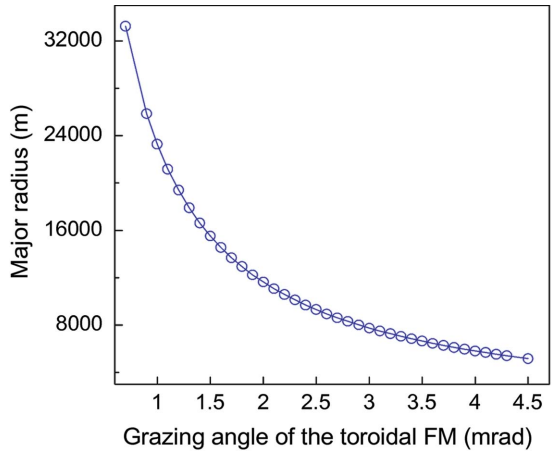

Figure 3
Major (meridional) radius as a function of the grazing incident angle. The vertical image distance is taken at 16.5 m from the toroidal FM. Since the major radius of the toroidal mirror is constrained to 11 km, the grazing incident angle of the current mirror is limited to 2 mrad.

increases. Based on these results, it is clear that we can achieve better focusing conditions (especially in the horizontal direction) at higher grazing angle, but for grazing incident angles above 3 mrad the vertical image distance exceeds 30 m, which is far away from the limited space of the beamline. In addition, the choice of the grazing angle for the toroidal mirror will be constrained by the mechanical limit of the mirror's major radius that can be changed between 11 and 33 km as can be seen in Fig. 3. Using the toroidal FM itself, one cannot achieve a beam size of less than 100 μm (H) and 13 μm (V), which is not sufficient for experiments under extreme conditions.

In order to decide the best way of combining the toroidal FM and the KB mirrors in tandem for better focusing at the sample position, it is important to discuss all other options for focusing the entire undulator beam by the toroidal FM. Obviously, in Fig. 2 the horizontal and vertical images are located at different positions when the toroidal FM is detuned by changing the grazing angle. One other option is to focus both the horizontal and vertical image distances at the same point. For this special case, the horizontal and vertical spot sizes (FWHM) of the toroidal FM mirror as a function of the grazing incident angle are shown in Fig. 4. From equations (1) and (2), the relation between the major radius and the minor radius of the mirror is given by

$$\rho = R\sin^2\theta. \tag{3}$$

For the existing toroidal FM mirror at sector 3 of the APS, the minor radius is fixed at 46 mm and the major radius can take any value from 11 to 33 km. Although in this specific case we achieve better focusing conditions at higher grazing angle, the major radius is required to be less than 11 km for angles above 2 mrad, which does not match with the range for the major radius of the existing toroidal FM as shown in Fig. 3. In this case, image distance is limited to 16 m or higher. This 16 m (55.5 m from the source) is just 1 m before the end of the C-station. For some applications, a slit system is required to make the beam size even smaller at the toroidal FM focal point, so it becomes easier to establish the required beam size at the sample position after it combines with the KB mirrors.

In order to focus the new images of the toroidal FM, it was suggested that the most sensible design is to utilize a set of KB mirrors placed just before the sample (Huang *et al.*, 2008; Heald, 2002). The combination of these two types of mirrors is a versatile method for focusing. There are two possible arrangements that can be used to combine the toroidal FM and KB mirrors. We can focus the toroidal FM either behind or in front of the sample position. In the first case, the KB mirrors are used to focus a virtual image after the mirror site. Such an arrangement is already used to focus the beam in the C-station for momentum-resolved high-energy resolution inelastic X-ray scattering experiments (Alatas *et al.*, 2011). In the second case, the KB mirrors are used to focus a real image in front of the mirror site. In both cases, the KB mirrors arrangement can focus independently in the horizontal and vertical directions. The KB mirrors reduce the image created by the toroidal FM by different demagnification ratios (f3/f4) in the horizontal and vertical directions, where f3 and f4 are source and image distances for the KB mirrors (Heald, 2002). We set the working distance of the KB mirrors (distance between the sample and the edge of the horizontal KB mirror) in the range between 100 mm and 500 mm. In fact, a 100 mm working distance is sufficient for IXS experiments under ambient conditions, while a ∼500 mm working distance is required for experiments under high pressure and at low temperature.

Another important factor we need to keep in mind for this design is the beam efficiency (the number of photons that can be collected) (Peatman, 1997; Huang *et al.*, 2008). Here the KB mirrors' length, the working distances and the grazing incident angle at the KB mirrors are very important parameters. At sector 3 we have trapezoid-shaped vertical and horizontal KB mirrors with dimensions of 200 mm (length) and 7 mm (thickness) with a clean aperture 170 mm long and 10 mm

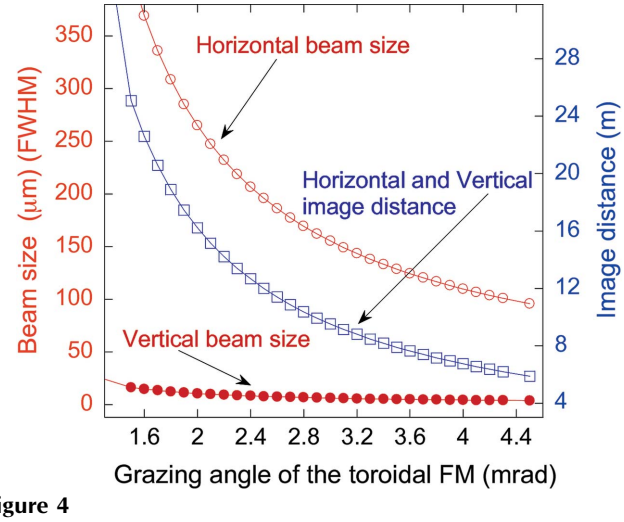

Figure 4
Horizontal and vertical image distance (blue open squares), and horizontal (red open circles) and vertical (red solid circles) spot sizes (FWHM) of the toroidal FM mirror, focused at the same image distance, as a function of the grazing incident angle.

wide. They are coated with Pd. The curvatures of the mirrors are adjusted by mechanical bending. For these KB mirrors, slope error and roughness are about 2.9 µrad and 3 Å r.m.s., respectively. Recently, another set of KB mirrors of lengths 300 mm (slope error of 0.89 µrad r.m.s.) and 200 mm (slope error of 0.39 µrad r.m.s.) have also been installed permanently at the C-station for IXS experiments. As mentioned before, the vertical beam size from the toroidal FM mirror is already sufficiently small and the 200 mm-long vertical KB mirror is capable of accepting almost all photons (with a transmission above 97%) for an ideal mirror. For the horizontal KB mirror, its length and/or grazing incident angle needed to be optimized. With this set-up, and if we chose to focus beam into the D-station, the 400 mm-long horizontal KB mirror is capable of accepting about 75% of photons for an ideal mirror. To be able to catch all photons and focus them in the horizontal direction, a longer horizontal KB mirror (about 800 mm) is required at the expense of deteriorating beam size. Smaller horizontal KB mirrors may be used with the upcoming upgrade of the APS of a multi-bent acromat (MBA) lattice for the ring that will give smaller beam size. Using combined optics, such as placing secondary focusing optics close to or exactly at the secondary source position, to maximize flux throughput for the microbeam and the general characteristics of the focusing as an alternative method is also under consideration (Huang *et al.*, 2010).

3. Ray-tracing and experimental results

Based on the above analyses (results shown in Figs. 2, 3 and 4), due to limited space at the beamline and considering the properties of the existing toroidal FM and KB mirrors at sector 3, we chose the following arrangements for microfocusing at the D- and E-stations.

For microfocusing at the D-station at the ^{57}Fe energy (14.41 keV), we chose a geometry such that the toroidal mirror focuses both the vertical and horizontal beam at the C-station (56 m from the source, 16.5 m from the toroidal FM). The grazing incident angle of the toroidal FM is chosen as 1.97 mrad. The horizontal KB mirror is placed at 300 mm; the vertical KB mirror is placed at 610 mm in front of the sample. The grazing incident angles of both KB mirrors are at 2.5 mrad. Expected beam profiles at certain positions are simulated by the ray-tracing software *SHADOW* (Lai & Cerrina, 1986; Sánchez del Rio & Dejus, 2004), including slope errors, and the results are shown in Fig. 5. We used the *WAVINESS* and *PREREFL* preprocessors of *SHADOW* to generate a random surface with different frequencies and slope errors, and roughness that matches the parameters of the existing mirrors. The existing toroidal mirror has a slope error of 5 µrad r.m.s., that broadens the image by about 2 × 5 µrad × 16.5 m = 165 µm r.m.s. at the toroidal FM focus point, and the KB mirrors that we used at the D-station have a slope

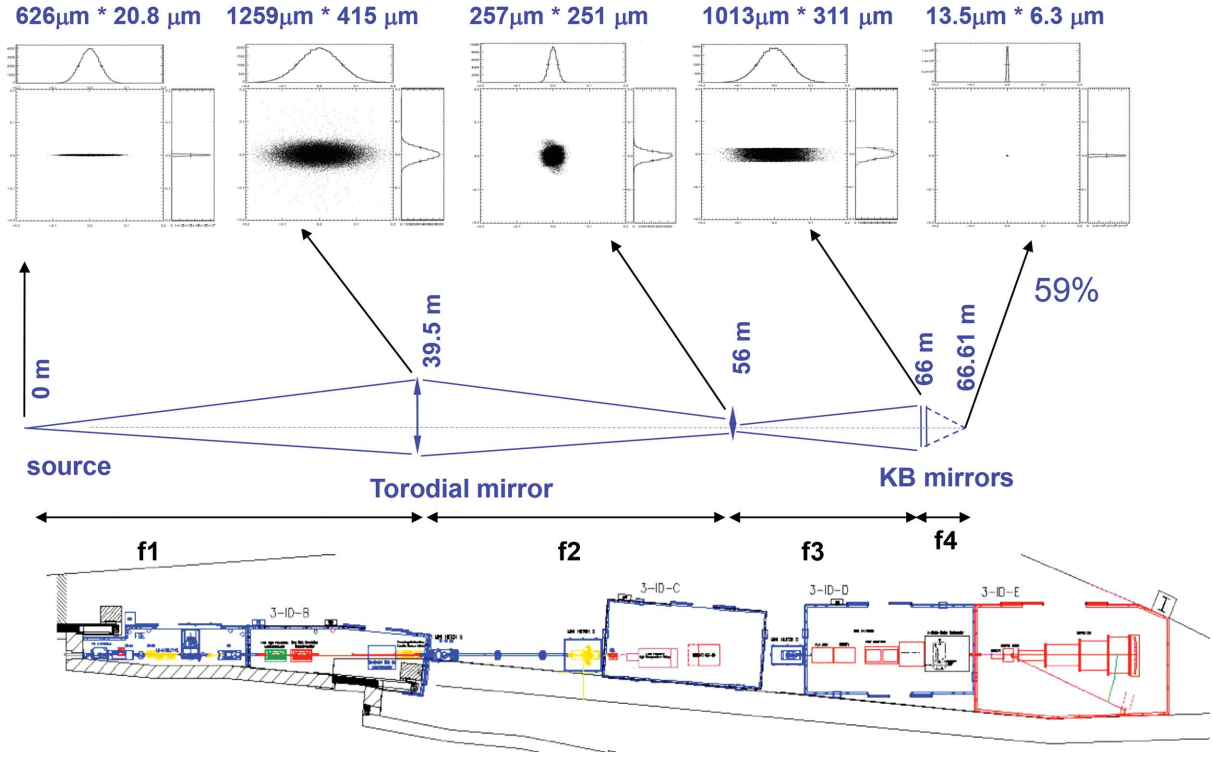

Figure 5
Schematic layout of the sector 3 beamline at the APS showing a combination of focusing elements (toroidal and KB mirrors) and their focal points at the D-station. f1 and f2 are the source and image distances for the toroidal mirror. f3 and f4 are the source and image distances for the KB mirrors. Beam sizes in their respective positions are simulated by the program package *XOP* in a 2 mm × 2 mm box to show the impact of the achieved focusing. Simulations presented in this figure were made considering the slope errors of the existing toroidal mirror and KB mirrors; the beam size grew from 4.5 µm (H) × 0.6 µm (V) to about 13.5 µm (H) × 6.3 µm (V) at the sample position.

error (2.9 µrad r.m.s.) that is actually quite large and has a considerable effect on the beam size. Including these slope errors, the beam size grows from 4.5 µm (H) × 0.6 µm (V) (FWHM) in the ideal case (*i.e.* without considering slope errors of the mirrors) to about 13.5 µm (H) × 6.3 µm (V) at the end of the D-station.

With the current technology in mirror fabrication, better mirrors can be produced with slope errors of less than 1 µrad. For a 0.5 µrad slope error for the KB mirrors, the slope error broadening in theory would be about 2 × 0.5 µrad × 0.300 m × 2.3548 = 0.7 µm FWHM for the horizontal KB mirror, and 2 × 0.5 µrad × 0.610 m × 2.3548 = 1.5 µm FWHM for the vertical KB mirror. Our *SHADOW* simulation values do not change too much for the 0.5 µrad slope error as compared with the ideal [about 5 µm (H) × 1 µm (V) (FWHM), which is quite similar to the values we found without errors]. Therefore, with better mirrors one can obtain a beam size of 5 µm (H) × 1 µm (V) or even sub-micrometer beam sizes in the vertical geometry easily by changing the existing mirrors that we use. In addition, the APS is restructuring an upgrade in terms of a new MBA lattice for the ring, which will reduce the horizontal emittance and effectively the horizontal beam size, and this will help the KB mirrors to focus at around the sub-micrometer level. With this, it might also be possible to use compound refractive lenses (CRLs) both in the vertical and horizontal directions with modification of the existing water-cooled diamond high-heat-load monochromators, that deteriorate the beam profile due to imperfections, to cryogenically cooled Si monochromators.

In Fig. 6 we have plotted the beam footprint at the toroidal, vertical and horizontal KB mirrors. For each mirror, we show (*a*) all rays, (*b*) good rays and (*c*) lost rays. As can be seen, the toroidal mirror is able to catch most of the photons; the number of lost rays is only 85 out of 5000 rays. Also, the 200 mm-long vertical KB mirror is capable of accepting almost all photons (the number of lost rays is only 95 out of 4915 rays). Most of the lost rays come from the horizontal KB mirror (the number of lost rays is 1187 out of 4820 rays). In our simulation, we choose the 400 mm-long horizontal KB mirror. To be able to catch all photons and focus them in the horizontal direction, a longer horizontal KB mirror (about 800 mm) is required. On the other hand, one should note that increasing the mirror length will increase the image-to-mirror distance, hence increasing the focal beam size. Another way to increase flux, albeit with increasing focal size, is to adjust the horizontal focusing of the toroidal mirror closer to the KB mirror, as demonstrated by Huang *et al.* (2010). The secondary source can even be on the KB mirror to maximize the throughput (Huang *et al.*, 2010). However, this option is constrained by the fixed location of the existing toroidal mirror. Instead of using a larger horizontal KB mirror at the D-station, multi-graded mirrors are under consideration to capture all available photons by increasing the reflection angle. Replacement of the toroidal mirror is also under

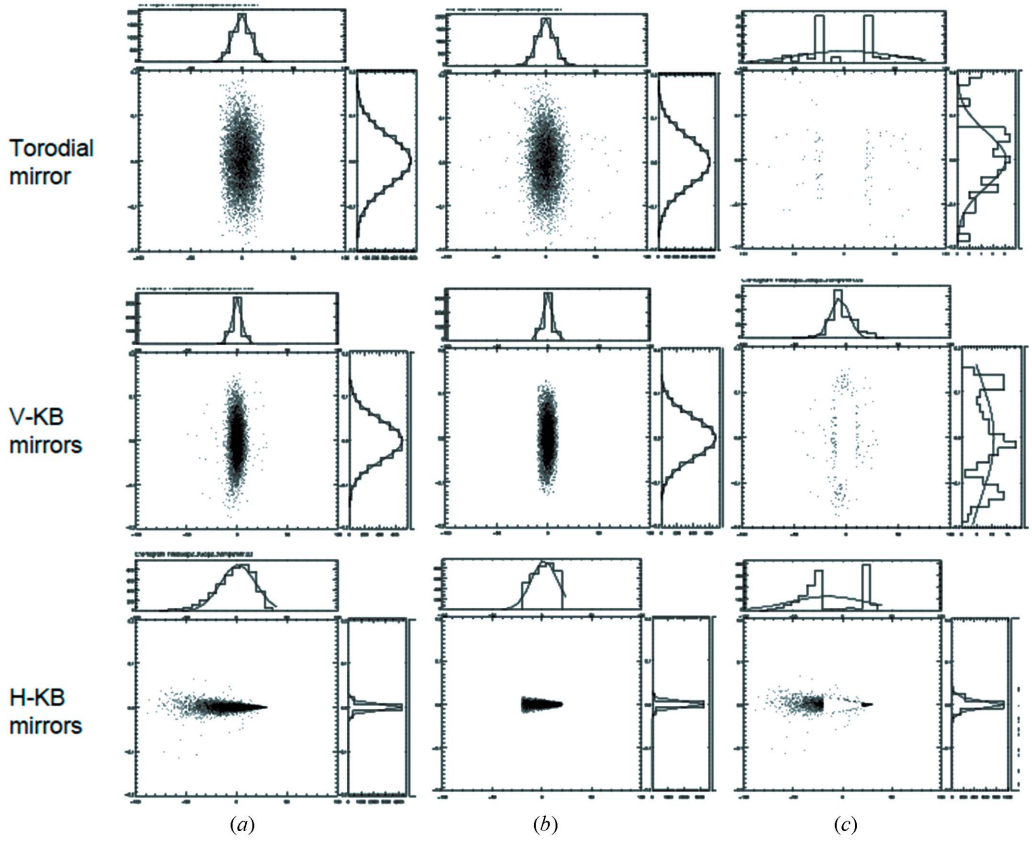

Figure 6
Beam footprint at the toroidal, vertical and horizontal KB mirrors. For each mirror, (*a*) all rays, (*b*) good rays and (*c*) lost rays are shown.

consideration with improved slope error and smaller bending radius. Graded mirrors or CRLs might be an option in the future depending on the final parameters of the proposed MBA lattice.

For microfocusing in the proposed E-station for sector 3, we choose a geometry such that the toroidal mirror focuses both the vertical and horizontal beam in the C-station (56 m and 56.205 m from the source). The grazing incident angle of the toroidal FM is selected to be 1.95 mrad. The horizontal KB mirror is placed at 300 mm and the vertical KB mirror is placed at 610 mm in front of the sample. The grazing incident angles of both KB mirrors are set to 2.5 mrad. Considering the slope errors of the existing toroidal mirror and KB mirrors, the beam size grows from 3.7 µm (H) × 0.46 µm (V) in the ideal case to 12.0 µm (H) × 6.0 µm (V) at the front-end of the proposed E-station (68 m from the source) with a transmission of up to 52%; the results are shown in Fig. 7.

In order to be more flexible regarding the options for the sample position, we simulated the spot size of the beam and the efficiency at different places in the D- and in the proposed E-stations. Fig. 8 shows the horizontal and vertical simulated spot sizes (FWHM) at the position of the sample as a function of the distance from the source (in the D-station). In Fig. 8(*a*) simulations were performed without consideration of the slope errors of both the toroidal mirror and KB mirrors, while in Fig. 8(*b*) simulations were performed with consideration of the slope errors of the existing toroidal FM and KB mirrors. The right-hand *y*-axis represents the efficiency of the beam at the position of the sample. Based on these results, it is clear that we could improve the focusing by increasing the distance from the source (because of the increase in the f3/f4 demagnification ratio), but the efficiency of the beam reduces. Simulations for the spot sizes at the proposed E-station (data not shown) show the same behavior with slight improvement in focusing because of the increase in the f3/f4 demagnification ratio, due to the focusing by increasing the distance from the source.

We tested our *SHADOW* ray-tracing simulations for microfocusing in the existing D-station and the results of the beam sizes are shown in Fig. 9. The beam profile is measured with a tungsten cylinder having a smooth surface, which is used to define a sharp edge. The best focus we achieved within experimental limitations was about 20 µm (H) × 12 µm (V) (FWHM) beam focal size at the sample position. Obviously, there is a slight difference between the measured and the calculated values [13.5 µm (H) × 6.3 µm (V)] based on the *SHADOW* ray-tracing simulations at the optimized parameters. Here, we should say that the above beam profile is measured with parameters that are slightly different from the optimized parameters suggested by the *SHADOW* ray-tracing

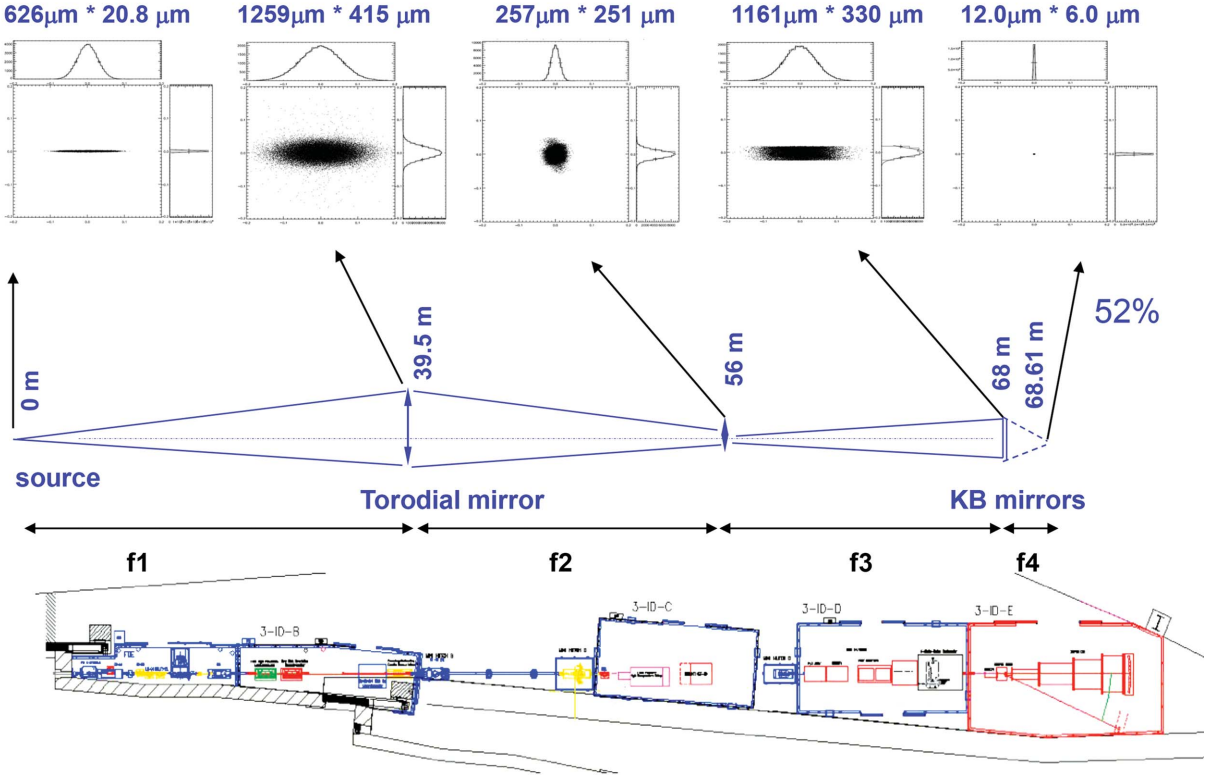

Figure 7
Schematic layout of the sector 3 beamline at the APS showing a combination of focusing elements (toroidal and KB mirrors) and their focal points at the proposed E-station. f1 and f2 are the source and image distances for the toroidal mirror. f3 and f4 are the source and image distances for the KB mirrors. Beam sizes in their respective positions are simulated by the program package *XOP* in a 2 mm × 2 mm box to show the impact of the achieved focusing. Simulations presented in this figure were made considering the slope errors of the existing toroidal mirror and KB mirrors; the beam size grows from 4.5 µm (H) × 0.6 µm (V) to about 12.0 µm (H) × 6.0 µm (V) at the sample position.

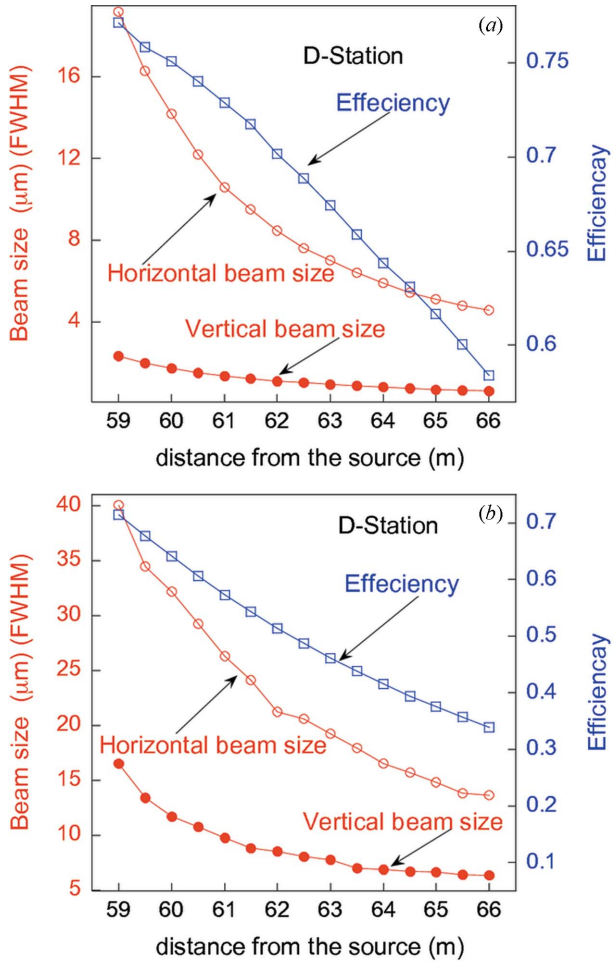

Figure 8
Horizontal and vertical simulated spot sizes (FWHM) at the position of the sample as a function of the distances from the source at the D-station. (*a*) Simulations were made without consideration of slope errors of both the toroidal mirror and KB mirrors. (*b*) Simulations were made with consideration of slope errors of the existing toroidal FM and KB mirrors. The right-hand *y*-axis represents the efficiency of the beam at the position of the sample (blue squares).

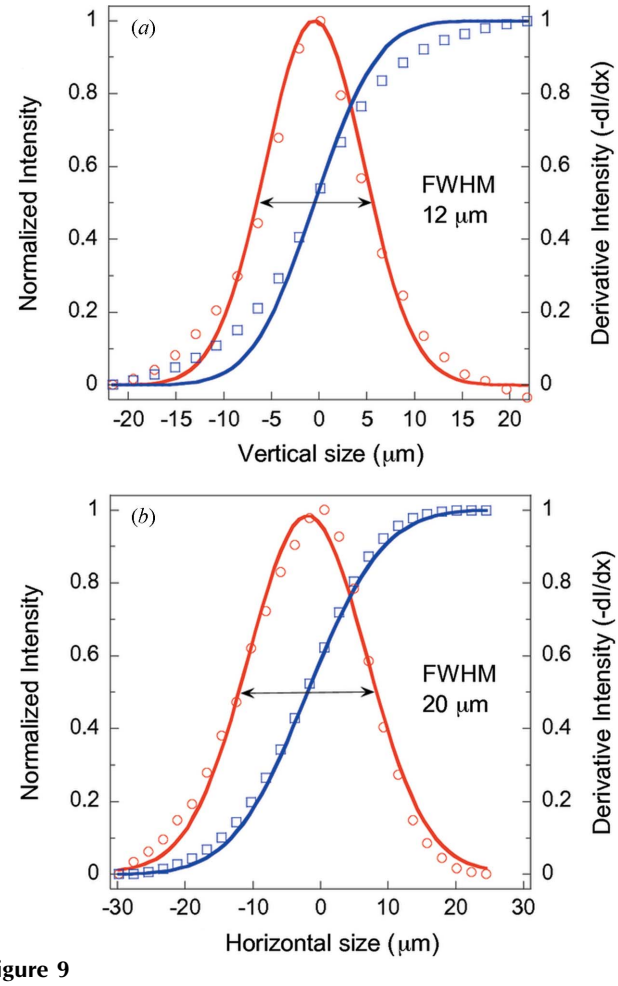

Figure 9
Measured vertical and horizontal beam size at the sample position at the D-station after using toroidal and KB mirrors in tandem. Red circles refer to the normalized intensity and blue squares represent the derivative intensity.

simulations. The beam profile is measured at the grazing angle of the toroidal FM of 1.6 mrad due to limited aperture of the beam transport lines, while for best focus the grazing incident angle of the toroidal FM is optimized to 1.97 mrad. The horizontal KB mirror is placed at 640 mm and the vertical KB mirror is placed at 850 mm in front of the sample during the measurement due to the experimental set-up. These values were optimized to 300 mm and 610 mm for best focus. Also, the grazing incident angles of both KB mirrors are optimized to 2.5 mrad for best focus and we used, for the measured beam profile, 2.4 mrad for the horizontal KB mirror and 2.2 mrad for the vertical KB mirror. In addition, the sample position for the measured beam profile was at 60.77 m from the source while the best focus was found at the end of the D-station, 66 m from the source. Finally, the beam profile is measured at the Eu nuclear resonance transition energy (around 21.54 keV), while for best focus we chose the ^{57}Fe nuclear resonance transition energy (around 14.24 keV). We repeated our *SHADOW* ray-tracing simulations with parameters that are used for the measured beam profile and obtained quite a good agreement between the measured 20 μm (H) × 12 μm (V) and the calculated 19.1 μm (H) × 9.7 μm (V) focal spot sizes.

Based on the above analysis, it is possible to achieve a beam spot size down to a few micrometers or even sub-micrometers for a possible upgrade project for sector 3 of the APS. The existing D-station and the proposed E-station will be more flexible for some optical elements rearrangement and in principle we can install new KB mirrors at the end of the D-station and anywhere in the E-station. However, other factors such as the placing of the cryostat, external magnets, monochromators and detectors need to be considered.

4. Conclusion

In conclusion, the combination of toroidal FM and KB mirrors was successfully applied to focus beam in the D- and proposed E-stations at sector 3 of the APS. Considering the slope errors of the existing toroidal FM and KB mirrors at sector 3, *SHADOW* ray-tracing simulations show that the combination of toroidal and KB mirrors at sector 3 of the APS can provide

beam sizes of 13.5 μm (H) × 6.3 μm (V) (FWHM) at the end of the D-station (66 m from the source) and of 12.0 μm (H) × 6.0 (V) (FWHM) at the beginning of the proposed E-station (68 m from the source). Therefore, with better mirrors, one can easily obtain a beam size of about 5 μm (H) × 1 μm (V) by changing the existing mirrors and by slight modification at the beamline with a transmission greater than 55%. Also under consideration is that the new proposed upgrade of APS in terms of the MBA lattice considered for the ring will bring new capability for effectively focusing the beam due to reduced emittance. It is possible to use CRLs in the vertical and/or horizontal directions for effective focusing.

We would like to thank the International Atomic Energy Agency (IAEA) for providing Dr A. M. Alsmadi with a supported fellowship to stay at the APS for six months during this project. Scientific discussions we have held with Dr Xianbo Shi and Ruben Reininger are acknowledged. Use of the Advanced Photon Source, an Office of Science User Facility operated for the US Department of Energy (DOE) Office of Science by Argonne National Laboratory, was supported by the US DOE under Contract No. DE-AC02-06CH11357.

References

Alatas, A., Leu, B. M., Zhao, J., Yavas, H., Toellner, T. S. & Alp, E. E. (2011). *Nucl. Instrum. Methods Phys. Res. A*, **649**, 166–168.
Bürck, U. van (1999). *Hyperfine Interact.* **123/124**, 483–509.
Burkel, E. (1991). *Inelastic Scattering of X-rays with Very High Energy Resolution.* New York: Springer.
Chumakov, A. I. & Sturhahn, W. (1999). *Hyperfine Interact.* **123/124**, 781–808.
Gao, L., Chen, B., Lerche, M., Alp, E. E., Sturhahn, W., Zhao, J., Yavaş, H. & Li, J. (2009). *J. Synchrotron Rad.* **16**, 714–722.
Heald, S. H. (2002). *Rev. Sci. Instrum.* **73**, 1527–1529.
Huang, C.-Y., Cai, Y. Q., Hiraoka, N., Chen, C.-C., Chung, S.-C., Song, Y.-F. & Tsang, K.-L. (2008). *J. Synchrotron Rad.* **15**, 50–54.
Huang, R., Meron, M., Kujala, N. & Barrea, R. A. (2010). *J. Synchrotron Rad.* **17**, 644–652.
Lai, B. & Cerrina, F. (1986). *Nucl. Instrum. Methods Phys. Res. A*, **246**, 337–341.
Mao, H. K., Kao, C. C. & Hemely, R. J. (2001*a*). *J. Phys. Condens. Matter* **13**, 7847–7858.
Mao, H. K., Xu, J., Struzhkin, V. V., Shu, J., Hemley, R. J., Sturhahn, W., Hu, M. Y., Alp, E. E., Vocadlo, L., Alfe, D., Price, G. D., Gillan, M. J., Schwoerer-Bohning, M., Hausermann, D., Eng, P., Shen, G., Giefers, H., Lubbers, R. & Wortmann, W. (2001*b*). *Science*, **292**, 914–916.
Mao, Z., Lin, J.-F., Liu, J., Alatas, A., Gao, L., Zhao, J. & Mao, H.-K. (2012). *Proc. Natl. Acad. Sci. USA*, **109**, 10239–10244.
Murphy, C. A., Jackson, J. M., Sturhahn, W. & Chen, B. (2001). *Geophys. Res. Lett.* **83**, L24306.
Peatman, W. B. (1997). *Grating, Mirrors and Slits.* Amsterdam: Gordon and Breach Science.
Sánchez del Rio, M. & Dejus, R. J. (2004). *Proc. SPIE*, **5536**, 171–174.
Sinn, H., Alp, E. E., Alatas, A., Barraza, J., Bortel, G., Burkel, E., Shu, D., Sturhahn, W., Sutter, J. P., Toellner, T. S. & Zhao, J. (2001). *Nucl. Instrum. Methods Phys. Res. A*, **467–468**, 1545–1548.
Sturhahn, W. (2004). *J. Phys. Condens. Matter* **16**, S497–S530.
Sturhahn, W. & Jackson, J. (2007). *Adv. High-Pressure Mineral.* **421**, 157–174.
Toellner, T. S. (2000). *Hyperfine Interact.* **125**, 3–28.
Toellner, T. S., Alatas, A. & Said, A. H. (2011). *J. Synchrotron Rad.* **18**, 605–611.
Toellner, T. S., Hu, M. Y., Bortel, G., Sturhahn, W. & Shu, D. (2006). *Nucl. Instrum. Methods Phys. Res. A*, **557**, 670–675.
Xu, S., Keefe, L. J., Mulichak, A., Yan, L., Alp, E. E., Zhao, J. & Fischetti, R. F. (2011). *Nucl. Instrum. Methods Phys. Res. A*, **649**, 104–106.
Yan, L., Zhao, J., Toellner, T. S., Divan, R., Xu, S., Cai, Z., Boesenberg, J. S., Friedrich, J. M., Cramer, S. P. & Alp, E. E. (2012). *J. Synchrotron Rad.* **19**, 814–820.
Zhao, J. Y., Alp, E. E., Toellner, T. S., Sturhahn, W., Sinn, H. & Shu, D. (2002). *Rev. Sci. Instrum.* **73**, 1611–1613.